Emergent large mechanical damping in ferroelastic-martensitic systems driven by disorder

Yan Ni,[1,*] Zhen Zhang,[1,†,‡] Minxia Fang,[1] Yanshuang Hao,[1] Xiangdong Ding,[1] Kazuhiro Otsuka,[2,§] and Xiaobing Ren[1,2,‡]

[1]*Multi-Disciplinary Materials Research Center, Frontier Institute of Science and Technology, and State Key Laboratory for Mechanical Behavior of Materials, Xi'an Jiaotong University, Xi'an 710049, China*

[2]*Center for Functional Materials, National Institute for Materials Science, Tsukuba, 305-0047 Ibaraki, Japan*

Disorders and point defects strongly interplay with the phase transition and alter the properties of ferroelastic-martensitic systems. Unusual static and quasistatic behaviors, such as time-dependent phase transitions, are discovered when disorders are introduced. However, the role of disorders on the ferroelastic system in vibrational environments at moderate frequency is rarely known, investigation of which could further shed light on their application as mechanical damping materials. Here we present the emergence of large damping capacity in ferroelastic-martensitic systems [including both the $Ti_{50-x}Ni_{50+x}$ alloy and $(Ca_{1-x}Sr_x)TiO_3$ ceramics] by introducing disorder (i.e., substitutional Ni and Sr, respectively). As the level disorder increases, the damping capacity of both systems raises and eventually reaches a maximum when long-range-ordered martensite tends to vanish. Moreover, near the disorder-induced phase boundary, we observe a large mechanical damping in ferroelastic ceramics $(Ca_{1-x}Sr_x)TiO_3$ with a figure of merit $\sim 2\,GPa^{1/2}$. Microscopic and dynamic investigations indicate that such damping plateau could result from the competing evolution of density and mobility of domain boundaries when disorder is introduced. Our work provides a degree of freedom to develop ferroelastic damping materials and a potential way to tune domain-boundary-mediated functionalities for other ferroic materials.

I. INTRODUCTION

Ferroelastic materials possess structural phase transition from high-symmetry parent phase to low-symmetry twin-related martensite phase [1,2]. The domain boundaries in martensite phase are movable under an external stress field, which enables the martensite state to accommodate large strain and gives rise to attractive functionalities such as shape memory effect and superelasticity [3–5]. Besides being used statically and in low frequencies, ferroelastic materials also possess interesting behavior in vibrational environments [6,7]. At moderate frequencies, ferroelastic-martensitic systems exhibit a broad mechanical damping peak due to the internal friction of domain boundaries and movable pinning centers [8,9]. Ultrahigh mechanical damping has been reported in the Ti-Ni-Fe alloy system due to the internal friction of domain boundaries and hydrogen [8]. Other than in ferroelastic alloys, the mechanical damping behavior is also observed in ferroelastic ceramics such as the Sr-doped $CaTiO_3$ perovskite and is attributed to the interaction between domain boundaries and oxygen vacancies [9]. Recent theoretical studies show that martensite systems can also dissipate vibration energy during the dynamical motion of domain boundaries [10]. The high-damping capacity in dynamic environments combined with relatively high strength enables ferroelastic-martensitic systems to be promising candidates for damping materials, which can be utilized to ensure the system's performance and lifetime by eliminating noise and vibration hazards [6,11,12]. It is also an important aspect for determining the operating frequency of multiferroic devices with a strong coupling to ferroelasticity [10].

In most situations of applying ferroelastic-martensitic materials, disorders and point defects (e.g., substitutional doping elements) are either introduced for achieving proper phase transition behaviors or involved inevitably during material synthesis [13,14]. It has been reported that disorders and point defects not only alter the phase transition and microstructure of materials but also lead to unusual properties and rich physics which are hardly obtained in pure systems [15–19]. Taking the prototype ferroelastic systems Ti-Ni shape memory alloy as an example, introducing a substitutional point defect such as Ni greatly reduces the martensitic transition temperature, increases the density of domain boundaries, and reduces the domain size, as well as introduces a state composed of nanosized martensite domains (termed as strain glass state) [13,20–22]. Moreover, fascinating phenomena are discovered along with the disorder-driven phase changes. Without possessing thermally driven martensitic phase transitions, shape memory effect and superelastic behaviors are reported in $Ti_{48.5}Ni_{51.5}$ strain glass state [23], and a time-dependent spontaneous martensitic phase transition is observed in $Ti_{48.7}Ni_{51.3}$ single crystals [24]. It is demonstrated that when disorder exists, a nontrivial competition between the thermodynamic landscape and the kinetic behavior of the ferroelastic system could arise.

---

*Present address: Seagate Technology LLC, Bloomington, Minnesota 55435, USA.

†Present address: School of Materials Engineering, Purdue University, West Lafayette, Indiana 47907, USA.

‡Corresponding authors: zhenn.zhang@gmail.com; ren.xiaobing@nims.go.jp

§Present address: 31-20, 2-chome, Umezono, Tsukuba 305-0045, Japan.

Although the above static and quasistatic behaviors of ferroelastic systems have been intensively studied by introducing the disorders and point defects, their role in the dynamical response of ferroelastic martensite, typically mechanical damping, is rarely known. Since mechanical damping is determined by the density as well as mobility of domain boundaries, disorder could bring about an unusual evolution of the mechanical damping behavior by changing the microstructure, phase stability, and kinetic behavior of ferroelastic-martensitic systems. Given that the highest electrostriction of ferroelectric systems (i.e., mechanical-electrical energy conversion under dynamic stimulation which is analogous to the mechanical-thermal energy conversion of ferroelastic damping) is usually observed in doped materials [25–27], disorders could also lead to the emergence of high mechanical damping in ferroelastic materials.

In the present work, we show with prototype ferroelastic materials such as $Ti_{50-x}Ni_{50+x}$ shape memory alloys and $Ca_{1-x}Sr_xTiO_3$ ceramics that a volcano-shaped evolution of mechanical damping emerges when disorders are introduced (i.e., substitutional elements Ni and Sr, respectively). The plateau of mechanical damping appears close to the disorder-induced phase boundary where martensitic transition vanishes. Near this critical region of disorder, mechanical damping of ferroelastic systems exhibits amplified sensitivity to the variation of an external field. These unusual behaviors of mechanical damping behavior could be attributed to the modification and competition of microstructure, kinetics of domain boundaries, and thermodynamic landscape of ferroelastic martensite upon introducing disorders. Moreover, we observe a large figure of merit of mechanical damping $\sim 2\,GPa^{1/2}$ in ferroelastic ceramics $(Ca_{1-x}Sr_x)TiO_3$, which is substantially higher than most bulk high-damping materials reported previously.

II. EXPERIMENT

A. Sample preparation

Disorder was introduced into the stochiometric $Ti_{50}Ni_{50}$ shape memory alloy by the substitution of Ti with Ni at the Ti site. $Ti_{50-x}Ni_{50+x}$ with $x = 0.0, 0.4, 0.5, 0.6, 1, 1.3, 1.5, 2,$ and 2.5 were fabricated by arc melting of high purity (>99.9%) Ti and Ni in argon atmosphere. In order to obtain a homogeneous distribution of excess Ni in the system, the samples were annealed in an evacuated quartz tube for 1 h at 1000 °C, followed by quenching in cold water.

Sr-doped $CaTiO_3$ ferroelastic oxide materials were utilized to further investigate the effect of disorder on mechanical damping capacity. $(Ca_{1-x}Sr_x)TiO_3$ with $x = 0.6, 0.7,$ and 0.8 (abbreviated as CST60, CST70, and CST80) were prepared by solid-state reaction method with starting materials of $CaCO_3$ (99.9%), $SrCO_3$ (99.9%), and TiO_2 (99.9%). The calcining was performed at 1300 °C in air for 6 h. The sintering was done at 1500 °C for 6 h followed by cooling in the furnace for 12 h.

B. Dynamical mechanical analysis

The damping behavior of samples was characterized by dynamic mechanical analysis (DMA) in the standard three-point bending mode. Damping capacity (indexed by $\tan\delta$)

and storage modulus (E) of $(Ca_{1-x}Sr_x)TiO_3$ samples were measured with applied vibration strain from $\varepsilon = 4.8 \times 10^{-5}$ to $\varepsilon = 0.6 \times 10^{-5}$ in the frequency range from 0.2 to 15 Hz. For $Ti_{50-x}Ni_{50+x}$, the vibration strain spans from $\varepsilon = 0.01\%$ to $\varepsilon = 0.12\%$. Stepwise isothermal measurement, unless otherwise noted, was utilized to eliminate the cooling/heating rate dependent transitory part of damping capacity, where the temperature step was set as 5 K with an isothermal time of 2 min. To compare with reported high-damping materials, the figure of merit to optimize both elastic modulus and damping capacity of materials was calculated as $E^{1/2}\tan\delta$ under bending condition [12].

C. Structural and microscopic characterization

In situ x-ray diffraction (XRD) measurement was carried out to study the structure change of Sr-doped $CaTiO_3$ samples upon thermal-driven phase transitions. The measurement was conducted on a Shimadzu XRD7000 diffractometer (Cu $K\alpha$ x rays) with a temperature-controlled sample holder from Anton Paar (TTK 450). The samples were isothermal for 30 min at each temperature before testing. The microstructure of Sr-doped $CaTiO_3$ under multiple doping concentrations was further investigated by transmission electron microscopy (TEM; JEM 2100F, JEOL). The samples for TEM observations were prepared by conventional methods such as mechanical grinding, cutting ultrasonically, dimpling, and ion milling.

III. RESULTS AND DISCUSSION

The evolution of mechanical damping of $Ti_{50-x}Ni_{50+x}$ as a function of excess Ni is shown in Fig. 1. Figure 1(a) shows the phase diagram of $Ti_{50-x}Ni_{50+x}$ where the martensitic transition temperature and phase boundaries are obtained from the temperature-dependent mechanical damping capacity ($\tan\delta$) curves shown in Figs. 1(b) and 1(c). The stoichiometric $Ti_{50}Ni_{50}$ possesses an ordered body-centered-cubic structure (B2) at high temperature (>350 K), representing an absence of point defects, such as excessive Ni [20]. At a low level of disorder ($x < 1.0$), the system transforms from parent phase to twin-related martensite phase [Fig. 1(a)]. For $Ti_{50-x}Ni_{50+x}$ with $x = 0.0, 0.5, 0.6$, two peaks appear upon cooling [Fig. 1(b)]. The peak appearing at higher temperature corresponds to the martensitic transition from the B2 parent phase to the B19′ martensite phase (marked as M_s). At a temperature lower than M_s (~ 200 K), another broad damping peak appears in these alloys [Fig. 1(b)], the peak temperature of which shifts with measurement frequency and can be fitted well with the Arrhenius relation (Supplemental Material Fig. S1 [28]). The activation energy is ~ 0.5 eV indicating that it is of relaxation type due to the interaction of domain boundaries and hydrogen [8,29]. We focus on the relaxation-type damping peak in this work since it appears in a broader temperature range, and the value of which is more stable against the change of frequency than the transition damping at M_s.

The relaxation-type damping capacity of $Ti_{50-x}Ni_{50+x}$ due to the domain boundary–hydrogen interaction exhibits clear dependence on the level of disorder. As Fig. 1(b) shows, the value of the damping peak increases from $\tan\delta \sim 0.02$ with $x = 0$ to $\tan\delta \sim 0.08$ with $x = 0.6$. The temperature
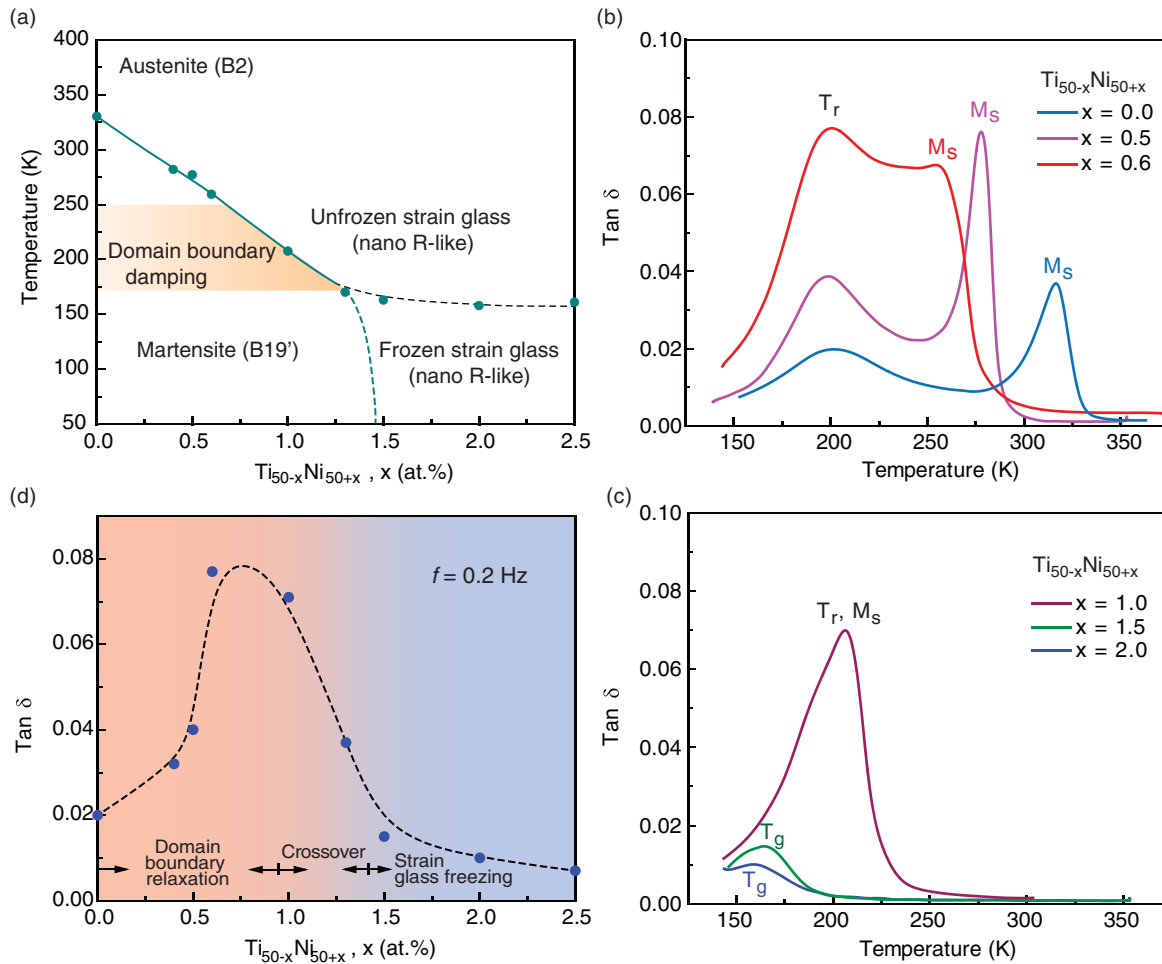
FIG. 1. Disorder-driven mechanical damping evolution of Ti-Ni ferroelastic shape memory alloys. (a) Phase diagram of Ti-Ni alloys as a function of Ni concentration obtained from mechanical damping (tanδ) vs temperature curves. (b) Temperature-dependent mechanical damping of $Ti_{50-x}Ni_{50+x}$ martensite ($x = 0.0$, 0.5, and 0.6). The relaxation-type damping peak at 200 K increases substantially with increasing excess Ni concentration. (c) Temperature-dependent mechanical damping of Ti-Ni in the crossover and strain glass regime ($x = 1.0$, 1.5, and 2.0), where opposite tendency is observed as the damping peak decreases when excess Ni increases. (d) The peak damping capacity as a function of excess Ni concentration, the value of which is obtained from domain boundary relaxation to strain glass freezing intermediated by a crossover region where domain boundary relaxation and martensitic transition merge together. The volcano-shaped dashed line is used as guidance.

of this mechanical damping remains almost constant under defect doping, indicating that the excess Ni does not alter the interaction of domain boundaries and hydrogen. The mechanical damping of $Ti_{50-x}Ni_{50+x}$ with a further increasing disorder level is shown in Fig. 1(c). $Ti_{50-x}Ni_{50+x}$ with $x = 1.0$ shows high mechanical damping with a peak value of tan $\delta \sim$ 0.75. The M_s temperature and domain boundary damping temperature T_r of this sample merge together (Supplemental Material Fig. S2 [28]). Successive suppression of mechanical damping is observed in $Ti_{50-x}Ni_{50+x}$ with $x = 1.5$ and 2.0. Their damping peak temperatures shift with measurement frequency and can be fitted with the Vogel-Fulcher relation (Supplemental Material Fig. S1 [28]), indicating that the mechanical damping of $Ti_{50-x}Ni_{50+x}$ with $x = 1.5$ and 2.0 results from the freezing of nanodomains (termed as strain glass transition) in this doping regime [16]. Figure 1(d) shows the mechanical damping of $Ti_{50-x}Ni_{50+x}$ as a function of excess Ni concentration x where a volcano-shaped variation is observed. The maximum value of mechanical damping

is >400% higher compared with that of both perfect and highly disordered samples. As the excess Ni concentration increases, the mechanism of damping changes from domain boundary relaxation to strain glass freezing (Supplemental Material Fig. S1 [28]), intermediated by a crossover region where domain boundary relaxation and martensitic transition overlap (Supplemental Material Fig. S2 [28]). The critical disorder level for the emergence of a mechanical damping plateau is $x \sim 0.75$, prior to the crossover region where the phase boundary between B19' martensite and strain glass state exists ($x \sim 1.3$).

The emergence of large mechanical damping upon disorder is further studied in prototype ferroelastic-martensitic ceramics $(Ca_{1-x}Sr_x)TiO_3$, where substitutional Sr acts to create disorder on the cation site. As Fig. 2(a) shows, doping Sr greatly reduces the cubic-tetragonal-orthodromic transition temperature. Similar to the Ti-Ni alloy, a precursor state with local clustering of octahedral tilts is reported in the cubic matrix above the transition temperature [30,31]. The mechanical damping of
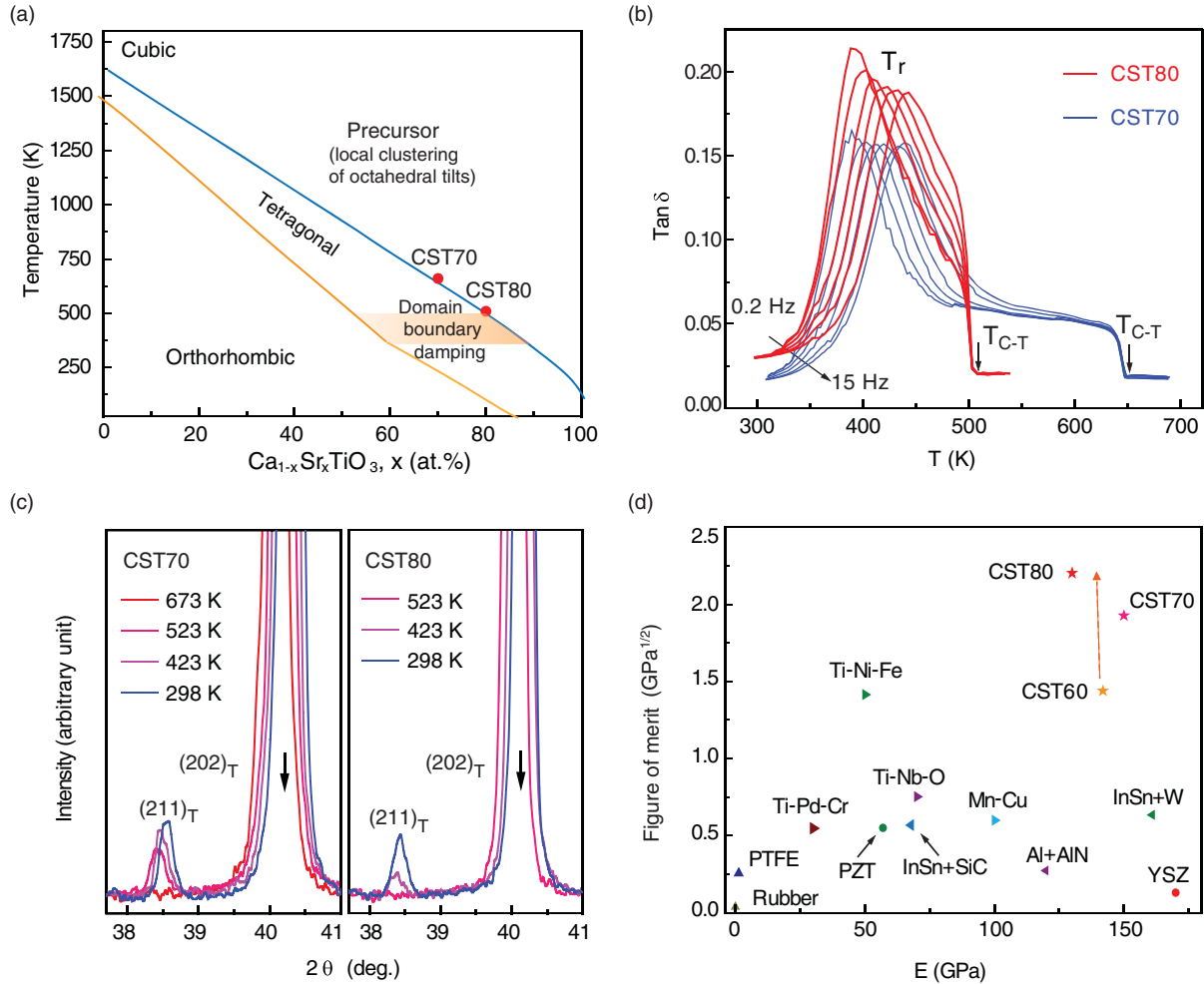
FIG. 2. Disorder-driven mechanical damping enhancement in Sr-doped $CaTiO_3$ ferroelastic perovskite. (a) The schematic transition phase diagram of $CaTiO_3$ as a function of Sr doping based on previous works [30,31]. The transition temperature of $(Ca_{1-x}Sr_x)TiO_3$ with $x = 0.7$ (CST70) and $x = 0.8$ (CST80) is measured from $\tan\delta \sim$ temperature curves and indicated by red spots. (b) Mechanical damping ($\tan\delta$) of CST70 and CST80 upon cooling. Relaxation-type damping peaks appear around 425 K. Substantial increase of mechanical damping appears in CST80, which possesses a higher level of disorders. (c) Temperature-dependent XRD profile of CST70 and CST80 in 2θ range from 37.5° to 41°, showing the cubic to tetragonal phase transition upon cooling. (d) Comparison on elastic modulus and figure of merit of high-damping materials. Sr doping increases the figure of merit of $(Ca_{1-x}Sr_x)TiO_3$, which fills the virgin area combining both high modulus and high mechanical damping.

$(Ca_{1-x}Sr_x)TiO_3$ with $x = 0.7$ (CST70) and $x = 0.8$ (CST80) as a function of temperature is shown in Fig. 2(b). For CST70, a stepwise increase of mechanical damping is observed at 650 K upon cooling. It corresponds to the cubic to tetragonal transition as evidenced by the appearance of a diffraction peak from the (211) plane of tetragonal phase [Fig. 2(c)] [32] and a step decrease of the storage modulus (Supplemental Material Fig. S3 [28]). With a further reduction of temperature, a frequency-dependent broad damping peak appears in CST70 with $\tan\delta \sim 0.15$ at $350-450$ K. The shifting of peak temperature with measurement frequency can be fitted well by the Arrhenius relation with activation energy of 1.2 eV (Supplemental Material Fig. S4 [28]), indicating that it is of relaxation type due to the interaction between domain boundaries and oxygen vacancies [9]. With increasing Sr doping to $x = 0.8$ [Figs. 2(b) and 2(c) and Supplemental Material Fig. S3 [28]], the cubic to tetragonal transition temperature decreases and approaches the relaxation damping peak. The tempera-

ture region for the relaxation damping remains the same for CST80 and CST70, indicating that the interaction between domain boundary and oxygen vacancies is not degraded by Sr (Supplemental Material Fig. S4 [28]). More importantly, a relaxation-type damping peak with maximum $\tan\delta \sim 0.2$ appears in CST80. Compared with the damping capacity of CST60 ($\tan\delta \sim 0.12$) (Supplemental Material Fig. S5 [28]), a substantial increase in mechanical damping of $(Ca_{1-x}Sr_x)TiO_3$ is observed with increasing the Sr doping level in the tetragonal state, which is similar to that observed in the martensitic region of the Ti-Ni alloy (Fig. 1). It therefore indicates the generality on the ability of disorder to substantially enlarge the mechanical damping of the martensite state.

Moreover, the figure of merit for the mechanical damping ($E^{1/2}\tan\delta$) [12] of CST70 and CST80 ferroelastic ceramics is outstanding when compared to various high-damping materials [Fig. 2(d)]. As shown in Supplemental Material Fig. S6 [28], a large damping capacity and high elastic modulus are usually
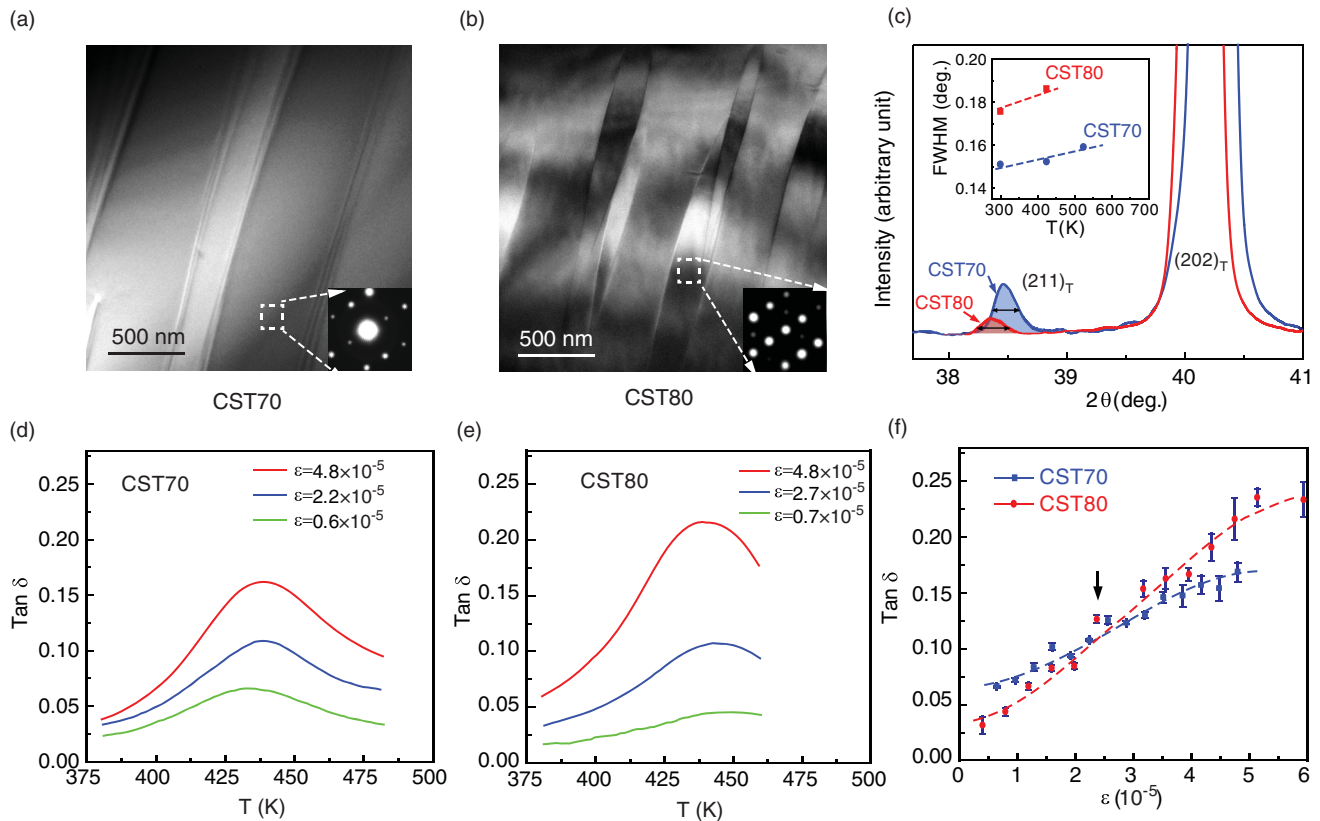
FIG. 3. Microscopic and dynamic behaviors of $(Ca_{1-x}Sr_x)TiO_3$ with $x = 0.7$ (CST70) and $x = 0.8$ (CST80). (a) and (b) Bright-field TEM images of CST70 (a) and CST80 (b) taken from the [110] direction (pseudocubic notation) of the tetragonal phase. The insets show the diffraction pattern in selected regions. The domain boundary density increases with disorders. (c) Comparison on the (FWHM of the $(211)_T$ x-ray diffraction peak of CST70 and CST80 at 423 K (tetragonal phase) obtained from Gaussian fit. The inset shows that CST80 possesses larger FWHM than CST70 in the temperature range of the tetragonal phase. (d) and (e) Mechanical damping as a function of vibration strain for CST70 (d) and CST80 (e). (f) Peak damping capacity as a function of vibration strain for CST70 and CST80. CST80 is more sensitive to the variation of vibration strain which gives rise to a crossover strain $\varepsilon = 2.5 \times 10^{-5}$. The nonlinearity in mechanical damping of CST70 and CST80 indicates the interplay between the vibration strain which drives domain boundaries to move and the disorder which restrains domain boundary motions.

hard for materials to possess simultaneously. Rubber and polymers possess a large damping capacity (>0.2), but their elastic modulus is less than 20 GPa [33,34]. Alloys (e.g., Ti-Pd-Cr, Mn-Cu, Ti-Ni-Fe, and Ti-Nb-O alloys) are another class of high-damping material [8,29,35,36]. They exhibit damping capacity ~ 0.1 on average with an elastic modulus of ~ 60 GPa, in which the Ti-Ni-Fe shape memory alloy shows the reported highest damping value as 0.2 [8]. Compared with polymers and alloys, ceramics [e.g., lead zirconic titanate (PZT) and yttria-stabilized zirconia (YSZ)] and some composites (e.g., InSn+SiC, Al+AlN, and InSn+W) possess the highest elastic modulus >100 GPa [33,37–39]. However, their damping capacity is low compared with alloy and polymers. It is therefore surprising that the CST80 and CST70 ceramics with high modulus of >120 GPa can exhibit mechanical damping which is larger than other ceramics such as PZT and YSZ and comparable to the Ti-Ni-Fe alloy. As Fig. 2(d) shows, the figure of merit of CST80 can reach ~ 2.0 GPa$^{1/2}$, which is beyond most of the reported bulk high-damping materials. Moreover, the figure of merit of bulk CST80 ceramics is significant when compared with that of the high-damping nanosized Cu-Al-Ni pillars (~ 1.0 GPa$^{1/2}$) and zirconia pillars (~ 2.0 GPa$^{1/2}$), the

damping of which attribute to the field-induced martensitic transitions [4,5]. Due to the transition nature of the Cu-Al-Ni and zirconia pillars, their damping mechanism can be utilized when the external strain exceeds the yield strains (for the zirconia pillar $\varepsilon_c > 3\%$ and for the Cu-Al-Ni pillar $\varepsilon_c > 1\%$) [4,5], which are ~ 200 times higher than the vibration strain applied here ($\varepsilon \sim 4.8 \times 10^{-5}$). As a result, the mechanical damping in CST80 and CST70 can fill the gap in applications with small vibrational noises.

To understand the disorder-induced large mechanical damping in the martensitic state, we further performed microscopic and dynamic investigations on CST70 and CST80 ferroelastic ceramics. Figures 3(a) and 3(b) show the representative bright-field TEM images of CST70 and CST80 at room temperature, both of which were taken from the [110] direction (pseudocubic notation) of the tetragonal phase. A domain structure is observed in both samples, which are generated by accommodating the lattice distortion associated with the cubic to tetragonal transition. Figures 3(a) and 3(b) further show that with increasing the level of disorder, the density of the domain boundary in CST80 becomes much higher than that of CST70. Moreover, we studied the domain boundary density of CST70

and CST80 in a larger measurement scale by extracting the full width at half maximum (FWHM) of the (211) diffraction peak of the tetragonal phase from their XRD profiles [Fig. 3(c)]. As the FWHM is inversely proportional to domain size [40], the larger FWHM observed in CST80 in the whole temperature region of the tetragonal phase [Fig. 3(c), inset] indicates its smaller domain size and larger domain boundary density, being consistent with the TEM observations.

The dynamic behavior of domain boundaries of ferroelastic martensite upon doping defects is studied by probing the variation of mechanical damping of CST70 and CST80 as the amplitude of vibration strain is changed. Figures 3(d) and 3(e) show the mechanical damping peak of CST70 and CST80 at 8 Hz, measured by heating up the samples continuously with a slow rate of 2 K/min. When $\varepsilon = 4.8 \times 10^{-5}$, CST80 shows a higher damping capacity (tan $\delta \sim 0.22$) than CST70 (tan $\delta \sim 0.17$), being consistent with Fig. 2(b). With reducing the vibration strain, the damping capacity of both CST70 and CST80 decreases. At the lowest vibration strain ($\varepsilon = 0.6 \times 10^{-5}$), the damping peak still exists for both samples. Interestingly, contrary to the damping value at high vibration strains, CST80 now possesses a lower damping capacity (tan $\delta \sim 0.03$) than CST70 (tan $\delta \sim 0.06$). A systematic study on the relation between the peak capacity of damping and vibration strain is shown in Fig. 3(f), where a crossover vibration strain $\varepsilon = 2.5 \times 10^{-5}$ is observed. Since CST80 possesses more domain boundaries than CST70, such a greater suppression of its mechanical damping at the low vibration strain indicates that the resistance on moving domain boundaries of CST80 is larger than that of CST70. We further studied the dynamic behavior of domain boundaries in $Ti_{50-x}Ni_{50+x}$ alloys, where a similar vibration strain induced crossover behavior of mechanical damping is observed in $x = 0.4$ and 0.6 (Supplemental Material Fig. S7 [28]). These results indicate the ability of disorders in ferroelastic martensite [$Ti_{50-x}Ni_{50+x}$ and $(Ca_{1-x}Sr_x)TiO_3$] to simultaneously increase domain boundary density and reduce domain boundary mobility.

A qualitative explanation on the emergence of large mechanical damping in a disordered ferroelastic martensite is shown in Fig. 4 schematically. As Fig. 4(a) shows, the ferroelastic martensite phase possesses a twin-related multidomain structure, which results from the symmetry-lowering martensitic transitions [2]. Due to the synergistical role of point defects on reducing the thermodynamic driving force to martensite and introducing a local stress field which favors short-range order [20,21,40], ferroelastic material with disorders (e.g., substitutional point defects Ni in Ti-Ni and Sr in CaSrTiO$_3$) transforms into the martensite state with smaller domain size and larger domain boundary density [Fig. 4(b)]. Such an effect of disorders on microstructure is observed in TEM images of CaSrTiO$_3$ ceramics [Figs. 3(a) and 3(b)] and also reported by theoretical calculations [21,40]. With a further increase in the level of disorder, the martensite phase is suppressed and nanodomains or clusters of martensite exist within the matrix of the parent phase [Fig. 4(c)] [16,30,41]. This corresponds to the disorder-induced phase boundary of Ti-Ni [Fig. 1(a)] and CaSrTiO$_3$ [Fig. 2(a)] where long-range-ordered martensite tends to vanish. The microscopic evolution of the ferroelastic materials with disorders therefore lead to an increase in domain boundary density as shown in Fig. 4(d). At the same time, the
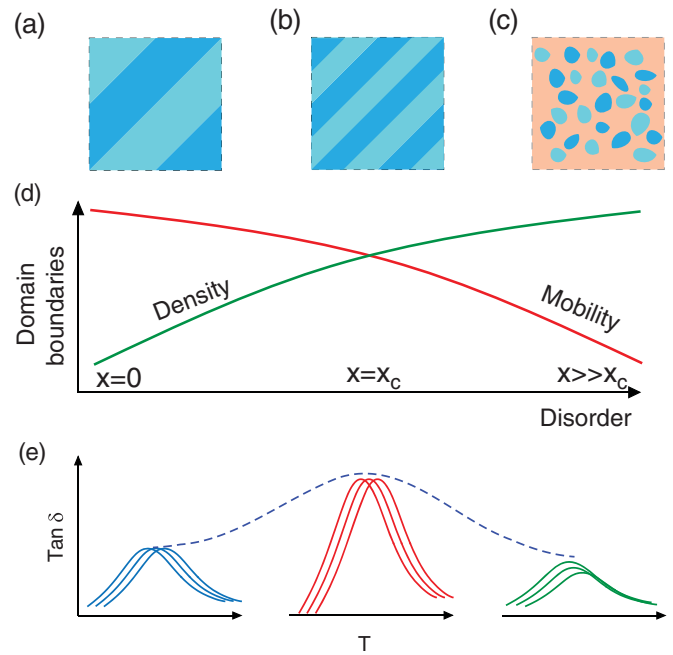
FIG. 4. Schematic relation of microstructure-disorder-mechanical damping of ferroelastic materials. (a)–(c) Microstructure of ferroelastic materials as a function of disorder, where the local field created by disorder hinders the coarsening of the martensite variant and eventually leads to the formation of a state with nanosized domains. (d) The evolution of domain boundary density and mobility as a function of disorder, where a crossover from the domain boundary density dominated region to the domain boundary mobility dominated region is observed at x_c. (e) Corresponding mechanical damping as a function of disorder, a maximum value of which appears near the disorder-induced crossover regime with a fine domain structure.

local stress field created by point defects introduces additional resistance to the motion of domain boundaries [Fig. 3(f)], which then results in the diminishing of the domain boundary mobility [Fig. 4(d)] under external field. Since the mechanical damping of ferroelastic martensite results from the internal friction of mobile domain boundaries with pinning centers (such as hydrogen in Ti-Ni and oxygen vacancies in CaSrTiO$_3$) in vibrational environments (Figs. 1 and 2), the crossover from the domain boundary density dominated region ($x < x_c$) to the mobility dominated region ($x \gg x_c$) in Fig. 4(d) can lead to the interesting disorder-driven evolution of mechanical damping as observed in Ti-Ni and CaSrTiO$_3$ [Figs. 1(d) and 2(b)]. As Fig. 4(e) shows, large mechanical damping appears near the crossover region by combining the large density and high mobility of domain boundaries, whereas the damping capacities of perfect and nanodomain martensite are limited by either low density or low mobility of domain boundaries. As a result, a volcano-shaped evolution of mechanical damping of ferroelastic martensite [Fig. 1(d)] appears with introducing disorders (e.g., point defects here).

The development of high-damping materials is crucially important for mechanical systems working in noisy environments. Several ferroelastic systems are studied as high-damping materials, and methods (such as reducing twining

shear [8,29]) have been developed to search high-damping ferroelastic systems. The present work not only demonstrates the utilization of disorder as an approach to induce large damping capacity in ferroelastic systems (e.g., Ti-Ni and CaSrTiO$_3$) but also indicates that great damping capacities could still be hidden in certain ferroelastic-martensitic systems until disorders are introduced. Moreover, in the physical parallel systems such as ferroelectrics, ferromagnetism, and multiferroics [42,43], there are important applications such as electrostriction, piezoelectric, magnetostriction, and magneto-electric, which rely on the dynamic response of their domain boundaries under external fields. The present work therefore demonstrates potential benefits for searching ultrahigh performance in these ferroic materials through the tunability of the dynamic response of domain boundaries by disorders.

IV. CONCLUSION

We have shown with prototype ferroelastic materials including Ti-Ni alloys and CaSrTiO$_3$ ceramics that disorders can strongly manipulate the behavior of the martensite state in dynamic environments. The mechanical damping of Ti-Ni alloys shows a volcano-shaped evolution as Ni defects are

introduced, and large mechanical damping is obtained in CaSrTiO$_3$ ceramics with substantial Sr doping. The plateau of mechanical damping appears close to the phase boundary where long-ranged martensite degrades. The emergence of large mechanical damping can be attributed to the ability of disorders to alter both the microstructure of the martensite state and the mobility of domain boundaries simultaneously. Moreover, a large damping figure of merit ($\sim$2.0 GPa$^{1/2}$) is obtained in (Ca$_{1-x}$Sr$_x$)TiO$_3$ ceramics with $x = 0.8$, which is outstanding among high-damping materials reported previously. Our work therefore shows that introducing disorders is a promising way to tune the dynamic response of ferroelastic materials and further sheds light on the development of other ferroic materials in dynamic environments.

[1] K. Otsuka and C. M. Wayman, *Shape Memory Materials* (Cambridge University Press, Cambridge, 1999).

[2] A. G. Khachaturyan, *Theory of Structural Transformations in Solids* (Courier Corporation, North Chelmsford, 2013).

[3] K. Otsuka and T. Kakeshita, MRS Bull. **27**, 91 (2002).

[4] J. S. Juan, M. L. No, and C. A. Schuh, Nat. Nanotechnol. **4**, 415 (2009).

[5] A. Lai, Z. Du, C. L. Gan, and C. A. Schuh, Science **341**, 1505 (2013).

[6] N. Igata, K. Nishiyama, K. Ota, Y. Yin, W. Wuttig, I. S. Golovin, J. V. Humbeeck, and J. San Juan, J. Alloys Compd. **355**, 230 (2003).

[7] W. L. Benard, H. Kahn, A. H. Heuer, and M. A. Huff, J. Microelectromech. Syst. **7**, 245 (1998).

[8] G. Fan, Y. Zhou, K. Otsuka, and X. Ren, Appl. Phys. Lett. **89**, 161902 (2006).

[9] M. Daraktchiev, R. J. Harrison, E. H. Mountstevens, and S. A. T. Redfern, Mater. Sci. Eng., A **442**, 199 (2006).

[10] Z. Zhao, X. Ding, T. Lookman, J. Sun, and E. K. H. Salje, Adv. Mater. **25**, 3244 (2013).

[11] A. D. Romig, Jr., M. T. Dugger, and P. J. McWhorter, Acta Mater. **51**, 5837 (2003).

[12] M. F. Ashby, *Materials Selection in Mechanical Design* (Pergamon, New York, 1992).

[13] K. Otsuka and X. Ren, Prog. Mater. Sci. **50**, 511 (2005).

[14] K. Otsuka and X. Ren, Intermetallics **7**, 511 (1999).

[15] X. Ren and K. Otsuka, Nature (London) **389**, 579 (1997).

[16] S. Sarkar, X. Ren, and K. Otsuka, Phys. Rev. Lett. **95**, 205702 (2005).

[17] T. Saito, T. Furuta, J.-H. Hwang, S. Kuramoto, K. Nishino, N. Suzuki, R. Chen, A. Yamada, K. Ito, Y. Seno *et al.*, Science **300**, 464 (2003).

[18] Y. Tanaka, Y. Himuro, R. Kainuma, Y. Sutou, T. Omori, and K. Ishida, Science **327**, 1488 (2010).

[19] X. Ren, Y. Wang, K. Otsuka, P. Lloveras, T. Castán, M. Porta, A. Planes, and A. Saxena, MRS Bull. **34**, 838 (2009).

[20] Z. Zhang, Y. Wang, D. Wang, Y. Zhou, K. Otsuka, and X. Ren, Phys. Rev. B **81**, 224102 (2010).

[21] D. Wang, Y. Wang, Z. Zhang, and X. Ren, Phys. Rev. Lett. **105**, 205702 (2010).

[22] J. Lu, G. T. Martinez, S. Van Aert, and D. Schryvers, Phys. Status Solidi **251**, 2034 (2014).

[23] Y. Wang, X. Ren, and K. Otsuka, Phys. Rev. Lett. **97**, 225703 (2006).

[24] Y. Ji, D. Wang, X. Ding, K. Otsuka, and X. Ren, Phys. Rev. Lett. **114**, 055701 (2015).

[25] S.-E. Park and T. R. Shrout, IEEE Trans. Ultrason. Ferroelectr. Freq. Control **44**, 1140 (1997).

[26] L. E. Cross, S. J. Jang, R. E. Newnham, S. Nomura, and K. Uchino, Ferroelectrics **23**, 187 (1980).

[27] W. Liu and X. Ren, Phys. Rev. Lett. **103**, 257602 (2009).

[28] See Supplemental Material at http://link.aps.org/supplemental/10.1103/PhysRevMaterials.2.053605 for additional figures.

[29] Y. Zhou, G. Fan, D. Xue, X. Ding, K. Otsuka, J. Sun, and X. Ren, Scr. Mater. **61**, 805 (2009).

[30] N. J. Perks, Z. Zhang, R. J. Harrison, and M. A. Carpenter, J. Phys.: Condens. Matter **26**, 505402 (2014).

[31] M. A. Carpenter, Am. Mineral. **92**, 328 (2007).

[32] A. T. R. Simon, J. Phys.: Condens. Matter **8**, 8267 (1996).

[33] D. D. L. Chung, J. Mater. Sci. **36**, 5733 (2001).

[34] R. S. Lakes, *Viscoelastic Materials* (Cambridge University Press, Cambridge, 2009).

[35] F. Yin, S. Takamori, Y. Ohsawa, A. Sato, and K. Kawahara, Mater. Trans. **43**, 466 (2002).

[36] F. Yin, S. Iwasaki, D. Ping, and K. Nagai, Adv. Mater. **18**, 1541 (2006).

[37] A. Bouzid, E. M. Bourim, M. Gabbay, and G. Fantozzi, J. Eur. Ceram. Soc. **25**, 3213 (2005).

[38] G. Roebben, B. Basu, J. Vleugels, and O. Van der Biest, J. Eur. Ceram. Soc. **23**, 481 (2003).

[39] Y. C. Wang, M. Ludwigson, and R. S. Lakes, Mater. Sci. Eng., A **370**, 41 (2004).

[40] P. Lloveras, T. Castán, M. Porta, A. Planes, and A. Saxena, Phys. Rev. B **80**, 054107 (2009).

[41] Y. Zhou, D. Xue, Y. Tian, X. Ding, S. Guo, K. Otsuka, J. Sun, and X. Ren, Phys. Rev. Lett. **112**, 025701 (2014).

[42] W. Eerenstein, N. D. Mathur, and J. F. Scott, Nature (London) **442**, 759 (2006).

[43] V. Wadhawan, *Introduction to Ferroic Materials* (CRC Press, Boca Raton, FL, 2000).